Effect of Surface Curvature on Contact Resistance between Abutting Cylinders

A thesis submitted by

Michael Mayer

in partial fulfillment of the requirements for the degree of

Master of Science

in

Mechanical Engineering

Tufts University

May 2018

Adviser: Marc Hodes

Abstract

Due to the microscopic roughness of contacting materials, an additional thermal resistance arises from the constriction and spreading of heat near contact spots. Predictive models for contact resistance typically consider abutting semi-infinite cylinders subjected to an adiabatic boundary condition along their outer radius. At the nominal plane of contact an isothermal and circular contact spot is surrounded by an adiabatic annulus and the far-field boundary condition is constant heat flux. However, cylinders with flat bases do not mimic the actual geometry of contacts. To remedy this, we perturb the geometry of the problem such that, in cross section, the circular contact is surrounded by an adiabatic arc. When the curvature of this arc is small, our solution is semi-analytical. Then, we employ a series solution for leading-order (flat-base) problem and use Green's Second Identity to compute the increase in contact resistance without needing to resolve the temperature field. Complimentary numerical results for contact resistance span the full range of geometric parameters, i.e., contact fraction and protrusion angle of the arc. The results suggest as much as a 10-15% increase in contact resistance for realistic contacts for typical contact sizes and asperity slopes.

Acknowledgments

First off, I want to thank my advisor, Professor Marc Hodes, for his guidance and help throughout this project. He took a chance on a young, inexperienced student with a passion for applied mathematics and has been as patient and encouraging as I could have ever hoped. I will forever be grateful.

I would also like to thank my committee members Professor Xiaozhe Hu, my co-adviser, who I look forward to working with more as I commence my PhD, and Professor Erica Kemmerling, whose class on Fluid Dynamics got me hooked on Transport Phenomenon as a field.

Special thanks to Dr. Toby Kirk and Professor Darren Crowdy at Imperial College London for their input and help throughout the duration of this project.

To my labmates past and present: Georgios Karaminas, Jonah Kadoko, Hy Dinh, Vikram Krishnamachari, and Dan Kane; thank you.

Thanks also goes to my family and loved ones who have endured many a distracted moment when I get lost in my head pondering a problem.

Thank you to the people behind the scenes of the Tufts Computing Cluster, a resource that proved invaluable in the completion of this thesis. Finally, thanks must go out to the National Science Foundation and the Soft Material Robotics IGERT program at Tufts (Grant #1144591) which have provided my funding the last two years.

Contents

List of Figures

Lists of Tables

1 Introduction

Flux-based thermal resistance, R'', subsequently referred to as thermal resistance, is the temperature drop (ΔT), per unit heat flux (q'') in the direction of heat flow as per

$$R'' = \frac{\Delta T}{q''} \tag{1}$$

In general, it may capture multi-dimensional conduction and convection effects. In the elementary case of one-dimensional, steady-state, Cartesian heat conduction, it becomes

$$R''_{\mathrm{1D}} = \frac{L}{k} \tag{2}$$

where L is the length of the material through which heat conducts and k is its thermal conductivity. When conduction is multi-dimensional on account of the size and geometry of the heat source at the base of the domain, the total thermal resistance (R''_{t}), is based upon the *mean* heat flux $\bar{q}''$ through it and can be decomposed into

$$R''_{\mathrm{t}} = R''_{\mathrm{1D}} + R''_{\mathrm{sp}} \tag{3}$$

where R''_{sp} is the spreading resistance, i.e., the additional temperature drop (ΔT_{c}) *due to spreading or constriction* of isotherms per unit heat flux in the direction of heat flow. When the base of the domain is flat, it is expressed as

$$R''_{\mathrm{sp}} = \frac{\Delta T_{\mathrm{c}}}{\bar{q}''} \tag{4}$$

where $\Delta T_{\mathrm{c}} = \bar{T}_{\mathrm{source}} - \bar{T}_{\mathrm{source\ plane}}$ as per the chapter by Yovanovich in the *Handbook of Heat Transfer* [1]. The concept of spreading resistance on account of the width of a heat source being smaller than that of a semi-infinite, Cartesian domain is illustrated in Fig. 1 for an isoflux source as per a solution by Mikic [2].

For one-dimensional, steady-state, Cartesian heat transfer between solid materials 1 and 2, in the idealized limit where temperature continuity is imposed across a flat interface between them,

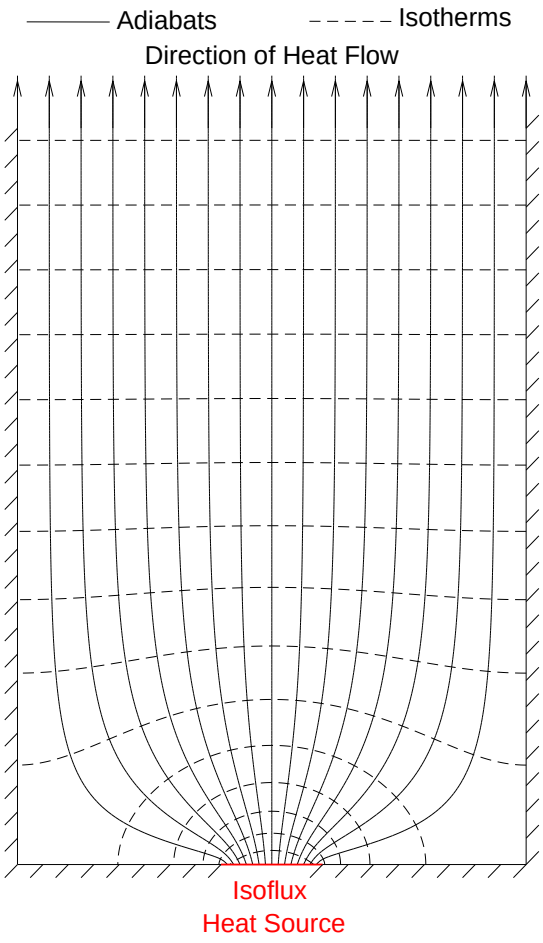

Figure 1: Isotherms (dashed curves) and adiabats (solid curves) for a two-dimensional temperature field when an isoflux heat source is of smaller width than the semi-infinite, Cartesian domain

the thermal resistance (R''_{ideal}) is

$$R''_{\text{ideal}} = \frac{L_1}{k_1} + \frac{L_2}{k_2} \tag{5}$$

This expression assumes temperature continuity at solid-solid interfaces. We note an additional resistance to heat flow resulting from the scattering of energy particles due to differences in the vibrational properties of the contacting materials may arise, yielding a temperature discontinuity; however, this resistance, known as Kapitza resistance, is assumed to be negligible in the above expression. In reality, the thermal resistance to heat transfer though the materials (R''_{real}) is

$$R''_{\text{real}} = \frac{L_1}{k_1} + \frac{L_2}{k_2} + R''_{\text{tc}} \tag{6}$$

where R''_{tc} is the thermal contact resistance, henceforth referred to as contact resistance. It captures the additional resistance to heat transfer that arises due to the roughness of real surfaces. A consequence of the roughness of real surfaces is that, typically, only 1-2% of the available surface area of two contacting surfaces is in physical contact, with the contact occurring only of the tips of asperities, leaving an interspatial gap for the vast majority of the available surface area. As the thermal conductivity of the interspatial fluid (typically air) is generally negligible compared to the thermal conductivity of the contacting materials, heat flowing between the two surfaces will constrict or spread to the contact points. This constriction and spreading gives rise to contact resistance and the phenomenon is depicted in Fig. 2 as per the solution by Crowdy [3] and discussed by Hodes *et al.* [4] in the context of contact resistance. When the lengths of materials 1 and 2 are large compared to the scale of the pitch of the contacts, as tends to be the case in real systems, contact resistance may be interpreted as a temperature discontinuity at the nominal plane of contact. The typical approach to the modeling of contact resistance is to use surface profiles and thermophysical properties of the contacting materials to develop a distribution of contact locations. This distribution is combined with spreading resistances expressions that arise from the modeling of a single contact. Because of this, much research has been done on the modeling of single contacts, our focus here.

Considering heat conduction between geometrically-identical contacting materials not neces-

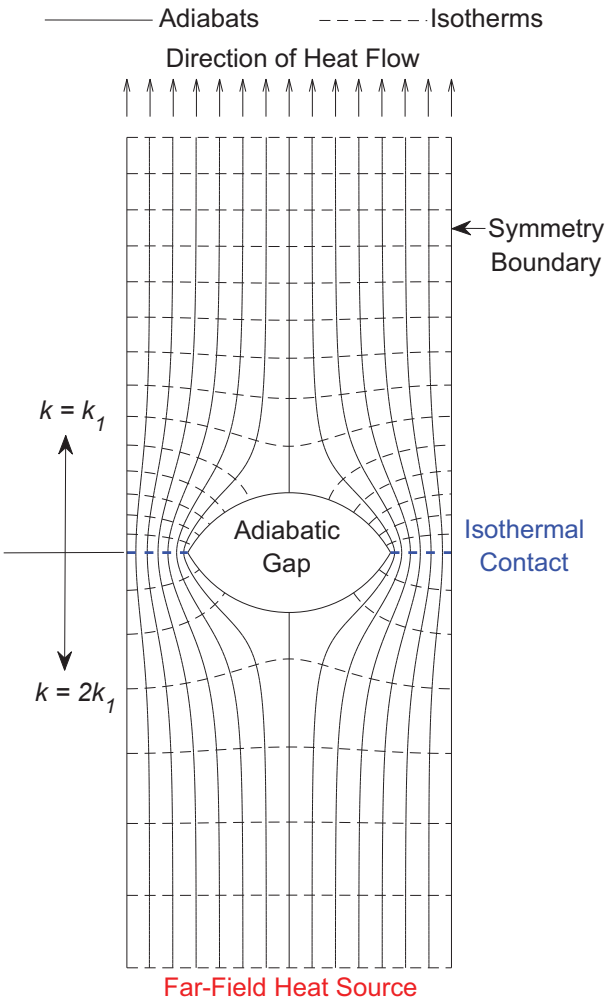

Figure 2: Illustration of contact resistance in Cartesian-geometry domain with materials of differing conductivities.

sarily of equal thermal conductivity, it follows from the symmetry arguments discussed in Cooper *et al.* [5] and generalized by Das and Sadhal [6] that the contact regions are isothermal. Thus the contact resistance problem reduces to a spreading resistance one. Decomposing the temperature field in an arbitrary spreading domain with isothermal contact spot into a one-dimensional (1D) and perturbative (p) part, Eq. (3) becomes

$$\overbrace{\frac{T_{\text{source}} - T_\infty}{\bar{q}''}}^{R''_{\text{t}}} = \overbrace{\frac{T_{\text{1D,source}} - T_{\text{1D},\infty}}{\bar{q}''}}^{R''_{\text{1d}}} + \overbrace{\frac{T_{\text{p,source}} - T_{\text{p},\infty}}{\bar{q}''}}^{R''_{\text{sp}}} \tag{7}$$

where T_{source} is the total source temperature in the problem. $T_{\text{1D,source}}$ and $T_{\text{p,source}}$ are the temperatures on the source of the 1D and perturbative problems after the problem has been decomposed as per Eq. 3.$T_{\text{1D},\infty}$ and $T_{\text{p},\infty}$ are those far from the source plane in the 1D and perturbative problems, respectively. We then get a solution for spreading resistance in an arbitrary domain such that

$$R''_{\text{sp}} = \frac{\Delta T_{\text{c}}}{\bar{q}''} = \frac{T_{\text{source}} - T_{\text{1D,source}}}{\bar{q}''} - \frac{T_\infty - T_{\text{1D},\infty}}{\bar{q}''} \tag{8}$$

This definition gives a means of calculating the spreading resistance in a contact with arbitrary shape by either specifying a temperature drop and solving for heat flux, or vice versa. In the case of a flat contact with isothermal contact spot, the perturbative problem has no average temperature and thus disappears as $z \to \infty$, restricting $T_\infty = T_{\text{1D},\infty}$ and yielding $\Delta T_{\text{c}} = T_{\text{source}} - \bar{T}_{\text{source}}$ as discussed before.

Contact resistance for single contacts is well documented in the literature. We note that for rectangular and circular-cross section domains, we refer to flux channels, defined as a rectangular flow channel with constant average heat flux throughout the domain, and flux tubes respectively. Cooper *et al.* [5] solve the canonical problem for the spreading resistance in a semi-infinite flux tube with a circular isothermal source surrounded by an adiabatic annulus along its base. A heat flux distribution resulting in an almost isothermal source was used to avoid a mixed boundary condition along the base of the domain and the results are accurate to within 2% for contact radius to cylinder radius ratios up to 40%. Mikic *et al.* [2] supported and expanded on the results from [5],

developing results for contact resistance in flux tubes with constant heat flux at the source, as well as solving for contact resistance in flux channels with various contact spot boundary conditions. Negus and Yovanovich [7] used a superposition of flux distributions to extend the results of [5] to higher ratios of contact radius to cylinder radius. Hunter *et al.* [8] discretized the integral equations developed by Sneddon [9] to solve for spreading resistance in a flux tube for a *true* isothermal contact, solving for the so-called constriction alleviation factor, also called constriction resistance parameter, from which spreading resistance follows. The analysis of these authors and the vast majority of subsequent ones assume a flat plane of contact. This is in contrast to the topography of real surfaces, in which micro-scale roughness is relevant.

Modelling for contact resistance generally uses values of the average height and slope of the asperities on contacting surface to define a relationship between the distribution and size of contacts to load pressures between contacting surfaces and hardness of the materials as per models by Cooper *et. al* [5] and Greenwood and Williamson [10]. The height and slope values can be captured through surface topography measurement techniques such as profilometry or taken from the mean square roughness values for the the manufacturing technique used in creation of the contacting surfaces. These distributions are coupled with spreading resistance expressions from simplified models of single contacts with a flat plane of contact as discussed above. Combined they give a model for contact resistance on a macro-scale. We develop spreading resistance expressions for non-flat contacts that better mimic the topology of real surfaces, and thus, when integrated into existing models, can give a better estimation of the contact resistance between contacting surfaces. As contact resistance is particularly important for contacting materials with high thermal conductivity, engineers can use our expressions to better design systems with applications from heat sinks for electronics packages to the cooling of nuclear reactors.

2 Previous Work

Instead of focusing on the non-flatness of contacts, later work has mainly focused on solving for spreading resistance assuming flat plane of contact increasing complexity, e.g., computing spreading resistance through stacks of thin materials as is often seen in microfluidics packaging appli-

cations. This is made clear by comprehensive reviews of spreading and contact resistance by Yovanovich [11] in 2005 and later Razavi [12] in 2016. Notably, however, some authors have examined the effect of non-flatness on single contacts. Madhusudana [13] used finite difference-simulation to quantify spreading resistance in conically-capped flux tubes. A flat, circular, isothermal source was placed at the truncated tip of a conical cap on a semi-infinite flux tube. They considered the cases in which the gap created by this conical cap was adiabatic and filled with a fluid of low thermal conductivity. Sano [14] analytically studied the effect of non-flatness on electrical contact resistance for a single contact by modeling the shape of the contact as a hyperboloid of one sheet. This enabled them to solve for spreading resistance in a non-flat halfspace. Das and Sadhal [6] considered the Cartesian-geometry problem for flat contacts between semi-infinite materials of different thermal conductivities adjacent to sparsely distributed, circular-arc geometry gaps, not assumed to be of equal protrusion angle, filled with a third material of finite thermal conductivity. Bipolar coordinates were used and further details are provided by Das [15] and Das and Sadhal [16]. Das and Sadhal [17] then used their solution to the single-gap problem as a basis for the (symmetric) multi-gap one to capture higher-order interactions between gaps. To preserve analytical tractability, it was further assumed that the gaps were thin, which simplified the temperature distribution in them and their interaction. The temperature field was computed to $O[(1-\gamma)^6]$, where γ is the contact fraction, from which the contact resistance follows, although the closed-form expression is not provided due to its length.

Notably, this paper was inspired, in part, by work done calculating apparent thermal and hydrodynamic slip lengths for flows over biomimetic superhydrophobic surfaces. For example, when both problems are made dimensionless, solving for the apparent hydrodynamic slip length in linear-shear flows in the Cassie state over parallel ridge-type superhydrophobic surfaces is identical to solving for thermal spreading resistance in Cartesian coordinates with an isothermal contact spot [18]. Indeed, solving for one immediately provides the result for the other [4]. As such, we are able to pull liberally from the robust literature on apparent slip lengths in the solution of our problem. The methodology and setup of the perturbation analysis in this paper is outlined by Sbragaglia and Prosperetti [19] and Lam *et al.* [20] in their work on apparent hydrodynamic and thermal slip,

respectively, along superhydrophobic surfaces.

Our goal is to capture the effect of the non-flat nature of real contacts on spreading resistance in a flux tube, where the correspondence with superhydrophobic surfaces no longer holds. We use a boundary perturbation of the solution of Hunter *et al.* [8] to model the annulus outside of the contact spot as an adiabatic-arc, rather than a flat one. The analysis follows the use of Green's Second Identity by Crowdy [21]. In using this technique, we find contact resistance to the first order in $\tilde{\varepsilon}$, where $\tilde{\varepsilon}$ is one half the dimensionless curvature of our arc, without fully resolving the correction to the temperature field due to boundary deflection. We quantify the increase in dimensionless contact resistance due to the curvature of the boundaries.

3 Methodology and Solution

We require the formulation of two problems, i.e., the temperature field of a flat contact T_0 as shown in Fig. 3a and that of a non-flat contact T as shown in Fig. 3b. Again, we only need to consider the spreading resistance problem from which contact resistance for a symmetric contact follows [6]. We define c as the contact radius, b as the cylinder radius, and $\phi = c/b$ as the constriction ratio. The contact angleα, is that between the tangent of the adiabatic-arc where it intersects the contact and the horizontal. It can be directly computed from knowledge of the average asperity slope of a surface. A positive contact angle corresponds to the arc penetrating into the solid, the relevant geometry for contact resistance.

For problems, T_0, and the non-flat contact problem, T, heat conduction is governed by the Laplace equation in axisymmetric, cylindrical coordinates.

$$\nabla^2 T_0 = \nabla^2 T = 0 \tag{9}$$

There is no singularity at $r = 0$, and an adiabatic boundary condition exists along the outside surface of the cylinder such that

$$\frac{\partial T_0}{\partial r} = \frac{\partial T}{\partial r} = 0 \quad \text{for} \quad r = 0, b \tag{10}$$

A constant heat flux leaves the domain as $z \to \infty$ as per

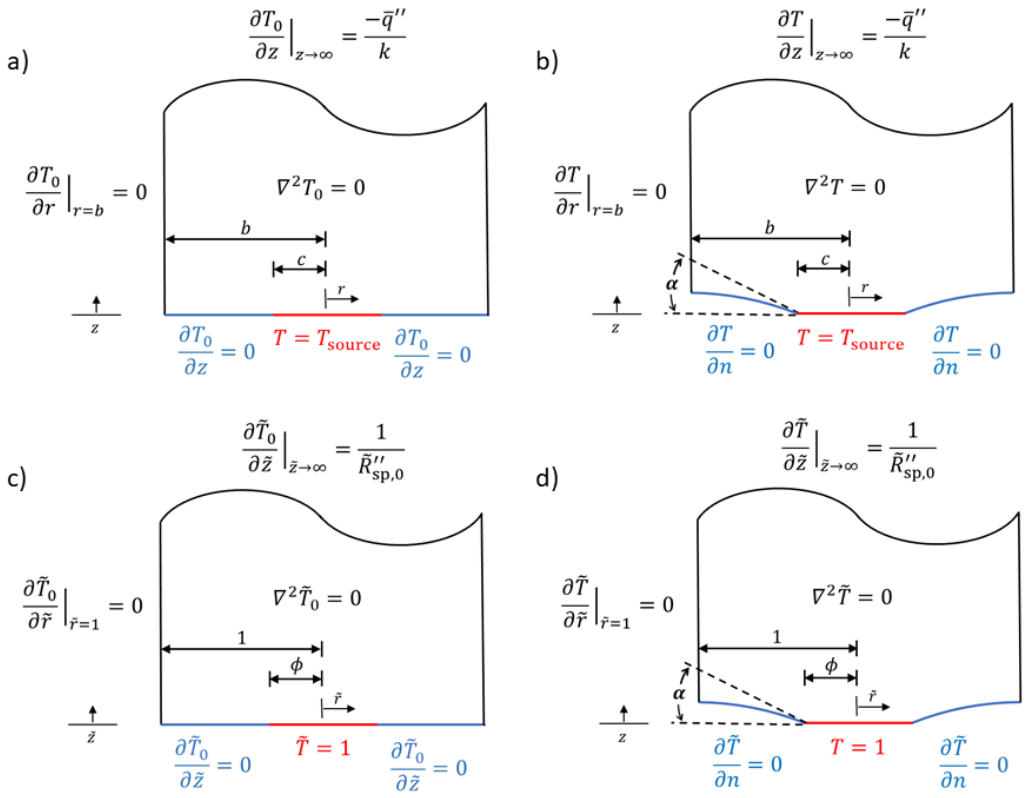

Figure 3: a) Dimensional flat contact problem. b) Dimensional non-flat contact problem. c) Dimensionless flat contact problem. d) Dimensionless non-flat contact problem.

$$\frac{\partial T_0}{\partial z} = \frac{\partial T}{\partial z} = -\frac{\bar{q}''}{k} \quad \text{for} \quad 0 < r < b, \quad z \to \infty \tag{11}$$

We prescribe an isothermal boundary condition at the contact spot such that

$$T_0 = T = T_{\text{source}} \quad \text{for} \quad 0 < r < c, \quad z = 0 \tag{12}$$

The adiabatic condition along the region outside the contact spot is

$$\begin{aligned} \frac{\partial T_0}{\partial z} &= 0 \quad \text{for} \quad c < r < b \\ \mathbf{n} \cdot \nabla T &= 0 \quad \text{for} \quad c < r < b \end{aligned} \tag{13}$$

where $\mathbf{n}$ is the normal vector to the adiabatic-arc.

3.1 Identification of the Small Parameter

Since the choice of the exact shape of the adiabatic surface is somewhat arbitrary, we choose to model the non-flat region outside of the contact spot such that it is circular in radial cross section. The shape of this circle, of radius R, is given by

$$z = \pm \left(\sqrt{R^2 - (r-b)^2} - \sqrt{R^2 - (b-c)^2} \right) \tag{14}$$

If we assume that R is large compared to b, i.e, $R/b >> 1$, then Taylor expanding the square roots yields

$$z = \pm \left(R \left[1 - \frac{1}{2} \left(\frac{r-b}{R} \right)^2 \right] - R \left[1 - \frac{1}{2} \left(\frac{b-c}{R} \right)^2 \right] \right) + O\left(\frac{b^3}{R^3} \right) \tag{15}$$

The $(+)$ sign corresponds to the arc protruding upwards as in Fig. 3b, while the $(-)$ sign corresponds to it protruding downwards and is relevant to spreading, but not contact resistance. We non-dimensional length by b and we place a tilde over our dimensionless quantities. The shape of our arc is defined as

$$\tilde{z} = -\tilde{\varepsilon}\tilde{\eta}(\tilde{r}) + O\left(\frac{1}{\tilde{R}^3}\right) \tag{16}$$

where $\tilde{\varepsilon}$ is a small parameter defined by

$$\tilde{\varepsilon} = \pm\frac{1}{2\tilde{R}} \tag{17}$$

and

$$\tilde{\eta}(\tilde{r}) = (\tilde{r}-1)^2 - (1-\phi)^2 \tag{18}$$

with $\phi = c/b$, the constriction ratio. Positive and negative $\tilde{\varepsilon}$ correspond to the arc protruding upward and downward, respectively. We note that $\tilde{\varepsilon}$ represents half the dimensionless curvature of the arc, and from geometry we find

$$\tilde{\varepsilon} = \frac{\sin(\alpha)}{2(1-\phi)} \tag{19}$$

Regarding thermal contact resistance, the fraction of the projecting area of mating surfaces in contact is typically 1%-2%. This corresponds to approximately $0.1 < \phi < 0.15$ therefore, even for an unrealistically high contact angle with magnitude 90 degrees, $\tilde{\varepsilon}$ is, at most, approximately 0.6.

3.2 Dimensionless Problem and Solution

In this section, we review the solution of Hunter *et al.* [8] which gives the dimensionless temperature field and dimensionless contact resistance of a flat contact. Then, we use reciprocity methods to find the dimensionless contact resistance of non-flat contacts without fully resolving the temperature field. We define the dimensionless temperature fields as

$$\tilde{T}_0 = \frac{T_0}{T_{\text{source}}}, \qquad \tilde{T} = \frac{T}{T_{\text{source}}} \tag{20}$$

and lengths are nondimensionalized by b. We choose our scheme to result in unit temperature at the source. The dimensionless problem formation for the flat and non-flat contact problems is shown in Figs. 3c and Fig. 3d, respectively. From Eq. (8), it is clear that solving for spreading resistance in a flux tube geometry requires specifying a temperature drop and solving for heat flux,

or vice versa. To solve the flat contact problem we do the former, calculating the dimensionless heat flux through a semi-infinite cylinder with a specified temperature drop due to constriction or spreading ($\Delta\tilde{T}_{0,\mathrm{c}}$) as per the next section. Later we assign this calculated heat flux to the non-flat contact problem to solve for the dimensionless temperature drop due to the combined effects of constriction or spreading and non-flatness ($\Delta\tilde{T}_{\mathrm{c}}$). $\Delta\tilde{T}_{0,\mathrm{c}}$ is given by $\Delta\tilde{T}_{0,\mathrm{c}} = \tilde{T}_{0,\mathrm{source}} - \bar{\tilde{T}}_{0,\mathrm{source\ plane}}$ since it is for a flat contact and $\Delta\tilde{T}_{\mathrm{c}} = (\tilde{T}_{\mathrm{source}} - \tilde{T}_{\mathrm{1D,source}}) - (\tilde{T}_{\infty} - \tilde{T}_{\mathrm{1D},\infty})$ as per Eq. (8) made dimensionless.

3.2.1 Flat Contact Problem

The governing equation is Laplace's Equation in axisymmetric $(\tilde{r},\tilde{z})$ cylindrical coordinates and the boundary conditions are the following. It follows from Eq. (**??**) and our subsequent prescription of mean temperature of zero along $z = 0$ that in the dimensional problem $\Delta T_{0,\mathrm{c}} = T_{\mathrm{source}}$, implying $R''_{\mathrm{sp}} = T_{\mathrm{source}}/\bar{q}''$. Then defining non-dimensional spreading resistance as $\tilde{R}''_{\mathrm{sp}} = R''_{\mathrm{sp}}k/b$, the boundary conditions on Laplace's equation in the dimensionless problem become

$$\tilde{\mathrm{z}} = 0 \quad \begin{cases} \tilde{T}_0 = 1 & 0 \le r < \phi \\ \frac{\partial \tilde{T}_0}{\partial \tilde{z}} = 0 & \phi < r \le 1 \end{cases} \tag{21}$$

$$\frac{\partial \tilde{T}_0}{\partial \tilde{z}} = -\frac{1}{\tilde{R}''_{\mathrm{sp}}} \quad \tilde{z} \to \infty \tag{22}$$

$$\frac{\partial \tilde{T}_0}{\partial \tilde{r}} = 0 \quad \tilde{r} = 1 \tag{23}$$

where $\tilde{R}''_{\mathrm{sp}}$ is unknown. Using separation of variables shown in Appendix A, the series solution which satisfies the homogeneous boundary on $\tilde{r} = 1$ and as $\tilde{z} \to \infty$ is

$$\tilde{T}_0(\tilde{r},\tilde{z}) = -\frac{1}{\tilde{R}''_{\mathrm{sp},0}}\tilde{z} + \sum_{n=1}^{\infty} \lambda_n^{-1} C_n J_0(\lambda_n \tilde{r}) \exp(-\lambda_n \tilde{z}) \tag{24}$$

where J_0 is a Bessel function of the First Kind and C_n are unknown coefficients. The eigenvalues λ_n satisfy $J_1(\lambda_n) = 0$. Applying Eq. (21) yields dual-series equations for C_n as

$$1 = \sum_{n=1}^{\infty} \lambda_n^{-1} C_n \mathrm{J}_0(\lambda_n \tilde{r}) \quad \text{for} \quad 0 \leq \tilde{r} < \phi \tag{25}$$

$$0 = -\frac{1}{\tilde{R}''_{\mathrm{sp},0}} - \sum_{n=1}^{\infty} C_n \mathrm{J}_0(\lambda_n \tilde{r}) \quad \text{for} \quad \phi < \tilde{r} \leq 1 \tag{26}$$

Sneddon [9] provides a semi-analytical means to solve a more general form of these dual-series equations. It follows from his result that, for the case at hand,

$$\tilde{R}''_{\mathrm{sp},0} = -\frac{1}{2\int_0^{\phi} h(t)\mathrm{d}t} \tag{27}$$

$$C_n = \frac{2}{\mathrm{J}_0^2(\lambda_n)} \int_0^{\phi} h(t)\cos(t\lambda_n)\mathrm{d}t \tag{28}$$

where $h(t)$ is defined as the solution to the integral equation

$$h(t) - \int_0^{\phi} h(u) G_1(t,u)\mathrm{d}u = \frac{2}{\pi} \tag{29}$$

where

$$G_1(t,u) = \frac{4}{\pi} + \frac{4}{\pi^2} \int_0^{\infty} \frac{K_1(y)}{yI_1(y)} [2I_1(y) - y\cosh(uy)\cosh(ty)]\mathrm{d}y \tag{30}$$

and I_1 and K_1 are first-order modified Bessel Functions of the First and Second Kind respectively. We discretize and evaluate the integrals numerically using quadrature. We invert the resulting matrix to determine the discrete values of $h(t)$ from which $\tilde{R}''_{\mathrm{sp},0}$ and C_n are computed via Eqs. (27) and (28). We note that for the flat contact problem it is not necessary to evaluate C_n; however, these coefficients are needed for the non-flat contact problem. Our spreading resistance results agree with the solution from [5] to within 2% for $0 < \phi < 0.4$, but diverge quickly as $\phi \to 1$, since their solution is valid only for $\phi << 1$, but ours is valid for the whole range, $0 < \phi < 1$.

3.2.2 Non-flat Contact Problem

Expressing the dimensionless temperature field for the non-flat contact problem, shown in Fig. 3d, as a Taylor series in $\tilde{\varepsilon} \ll 1$, it takes the form

$$\tilde{T}(\tilde{r},\tilde{z}) = \tilde{T}_0 + \tilde{\varepsilon}\tilde{T}_1 + O(\tilde{\varepsilon}^2) \tag{31}$$

where $\tilde{T}_0$ is the temperature profile assuming a flat adiabatic region outside the contact spot, i.e the flat contact problem, and $\tilde{T}_1$ is the change to the first order in $\tilde{\varepsilon}$ that results from the deflection of the boundary. The result is

$$\tilde{T} = -\frac{1}{\tilde{R}''_{\mathrm{sp},0}}\tilde{z} + \sum_{n=1}^{\infty} \lambda_n^{-1} C_n J_0(\lambda_n \tilde{r}) \exp(-\lambda_n \tilde{z}) + \tilde{\varepsilon}\tilde{T}_1 + O(\tilde{\varepsilon}^2) \tag{32}$$

Since the far field boundary condition is constant heat flux for $\tilde{T}'$, then as $\tilde{z} \to \infty$,$\tilde{\varepsilon}\tilde{T}_1$ must converge to a constant, denoted as $\Delta\tilde{T}_{\mathrm{p}}$ such that as $\tilde{z} \to \infty$, $\tilde{T}_\infty \to \tilde{T}_{1\mathrm{D},\infty} + \Delta\tilde{T}_{\mathrm{p}}$. Noting that in a not-flat contact with source temperature of 1 the temperature drop due to constriction or spreading is given by $\Delta\tilde{T}_{\mathrm{c}} = (1 - \tilde{T}_{1\mathrm{D,source}}) - (\tilde{T}_\infty - \tilde{T}_{1\mathrm{D},\infty})$, evaluated in this case as$\Delta\tilde{T}_{\mathrm{c}} = 1 - \Delta\tilde{T}_{\mathrm{p}}$.

It is convenient in the application of Green's Second Identity to have the source temperature in both problems be zero. To achieve this, we introduce dimensionless temperature fields $\tilde{T}'_0 = \tilde{T}_0 - \tilde{T}_{\mathrm{source}}$, and $\tilde{T}' = \tilde{T} - \tilde{T}_{\mathrm{source}}$, where $\tilde{T}'_0$ represents the flat contact problem with zero source temperature and $\tilde{T}'$ represents the non-flat contact one with zero source temperature. We now have two dimensionless temperature fields,

$$\tilde{T}'_0 = -\frac{1}{\tilde{R}''_{\mathrm{sp},0}}\tilde{z} + \sum_{n=1}^{\infty} \lambda_n^{-1} C_n J_0(\lambda_n \tilde{r}) \exp(-\lambda_n \tilde{z}) - 1 \tag{33}$$

$$\tilde{T}' = -\frac{1}{\tilde{R}''_{\mathrm{sp},0}}\tilde{z} + \sum_{n=1}^{\infty} \lambda_n^{-1} C_n J_0(\lambda_n \tilde{r}) \exp(-\lambda_n \tilde{z}) - 1 + \tilde{\varepsilon}\tilde{T}_1 + O(\tilde{\varepsilon}^2) \tag{34}$$

Then in the limit as $\tilde{z} \to \infty$,

$$\tilde{T}'_0 \sim -\frac{1}{\tilde{R}''_{\mathrm{sp},0}}\tilde{z} - \Delta\tilde{T}_{0,\mathrm{c}}$$

$$\tilde{T}' \sim -\frac{1}{\tilde{R}''_{\mathrm{sp},0}}\tilde{z} - \Delta\tilde{T}_{\mathrm{c}} + O(\tilde{\varepsilon}^2)$$

Note that the gradients remain unchanged in the above transformation and both are still governed by Laplace's equation. See Fig. 4 for an illustration of both problems. Green's Second Identity on the domain D of the non-flat contact domain, states that

$$\iiint_D \left(\tilde{T}_0'\nabla^2\tilde{T}' - \tilde{T}'\nabla^2\tilde{T}_0'\right)\mathrm{d}V = \oiint_{\partial D}\left(\tilde{T}'\frac{\partial\tilde{T}_0'}{\partial\hat{n}} - \tilde{T}_0'\frac{\partial\tilde{T}'}{\partial\hat{n}}\right)\mathrm{d}A \tag{35}$$

where $\hat{n}$ is the inward pointing unit normal. The volume integral disappears as both fields are governed by Laplace's Equation. Using the adiabatic boundary condition at $\tilde{r}=1$, zero temperature boundary condition at the source and adiabatic boundary condition along the meniscus and noting the derivatives for the prime functions are the same as in the original functions, this simplifies to

$$0 = \iint_{\tilde{z}\to\infty}\tilde{T}'\frac{\partial\tilde{T}_0}{\partial\hat{n}} - \tilde{T}_0'\frac{\partial\tilde{T}}{\partial\hat{n}}\mathrm{d}A + \iint_{\tilde{z}=-\tilde{\varepsilon}\tilde{\eta}}\tilde{T}'\frac{\partial\tilde{T}_0}{\partial\hat{n}}\mathrm{d}A \tag{36}$$

Evaluating the far-field integral yields

$$0 = \left[\left(-\frac{1}{\tilde{R}''_{\mathrm{sp},0}}\tilde{z} - \Delta\tilde{T}_{\mathrm{c}}\right) - \left(-\frac{1}{\tilde{R}''_{\mathrm{sp},0}}\tilde{z} - \Delta\tilde{T}_{0,\mathrm{c}}\right)\right]\frac{\pi}{\tilde{R}''_{\mathrm{sp},0}} + \iint_{\tilde{z}=-\tilde{\varepsilon}\tilde{\eta}}\tilde{T}'\frac{\partial\tilde{T}_0}{\partial\hat{n}}\mathrm{d}A \tag{37}$$

Plugging in for $\tilde{T}'$ results in

$$0 = \left(\Delta\tilde{T}_{0,\mathrm{c}} - \Delta\tilde{T}_{\mathrm{c}}\right)\frac{\pi}{\tilde{R}''_{\mathrm{sp},0}} + \iint_{\tilde{z}=-\tilde{\varepsilon}\tilde{\eta}}(\tilde{T}_0 + \tilde{\varepsilon}\tilde{T}_1 - 1)\frac{\partial\tilde{T}_0}{\partial\hat{n}}\mathrm{d}A + O(\tilde{\varepsilon}^2) \tag{38}$$

Leaving

$$\Delta\tilde{T}_{\mathrm{c}} - \Delta\tilde{T}_{0,\mathrm{c}} = \frac{\tilde{R}''_{\mathrm{sp},0}}{\pi}\iint_{\tilde{z}=-\tilde{\varepsilon}\tilde{\eta}}\left(\tilde{T}_0 + \tilde{\varepsilon}\tilde{T}_1 - 1\right)\frac{\partial\tilde{T}_0}{\partial\hat{n}}\mathrm{d}A + O(\tilde{\varepsilon}^2) \tag{39}$$

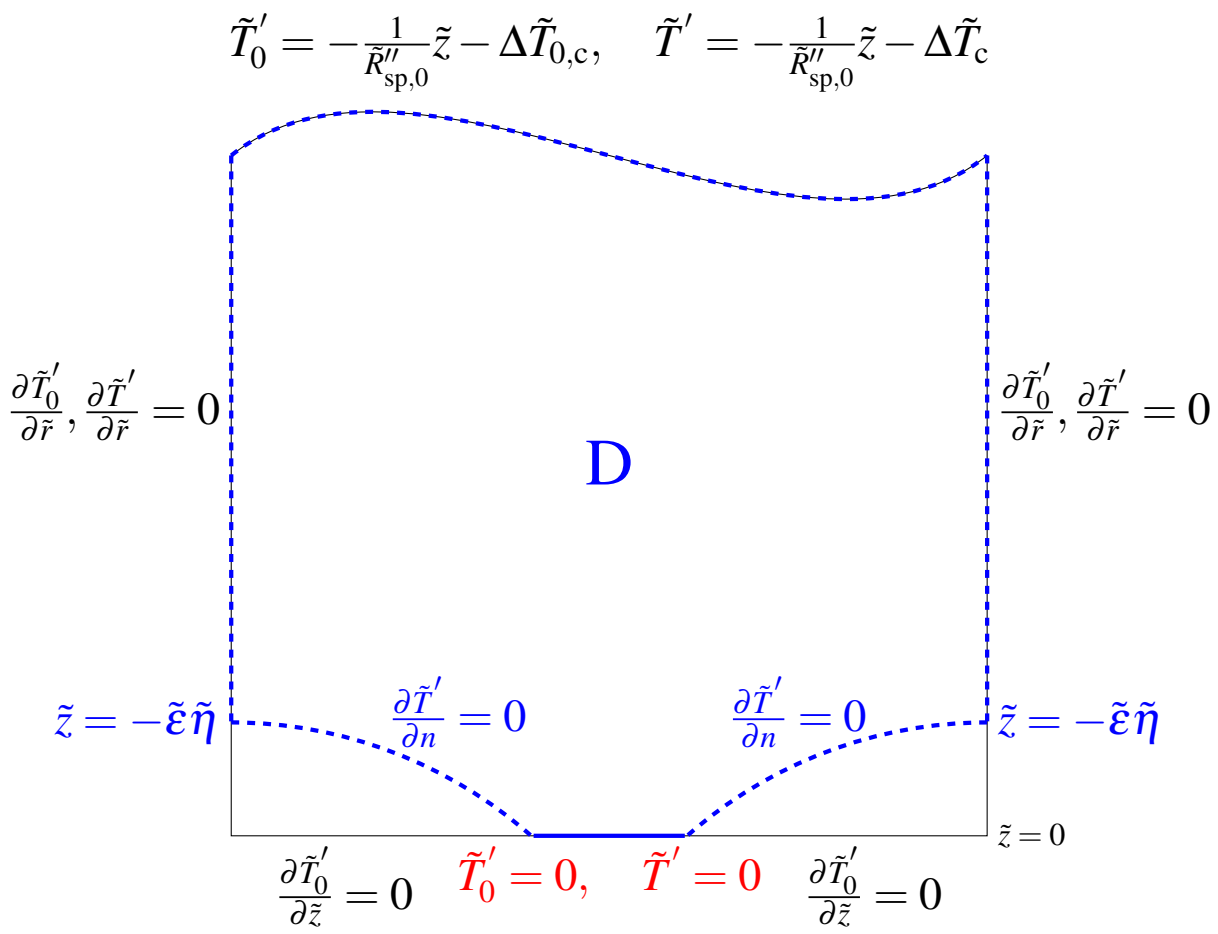

Figure 4: Domain D (dashed region) with all relevant boundary conditions

3.2.3 Linearizing Integrals along the Adiabatic-arc

Taking the outward facing unit normal vector as $\hat{n} = \frac{1}{|\mathbf{n}|}\left[\tilde{\varepsilon}(\mathrm{d}\tilde{\eta}/\mathrm{d}\tilde{r})\hat{\mathbf{r}} + \hat{\mathbf{z}}\right]$, then

$$\left.\frac{\partial\tilde{T}_0}{\partial\hat{n}}\right|_{\tilde{z}=-\tilde{\varepsilon}\tilde{\eta}} = \frac{1}{|\mathbf{n}|}\left(\tilde{\varepsilon}\frac{d\tilde{\eta}}{d\tilde{r}}\left.\frac{\partial\tilde{T}_0}{\partial\tilde{r}}\right|_{\tilde{z}=-\tilde{\varepsilon}\tilde{\eta}} + \left.\frac{\partial\tilde{T}_0}{\partial\tilde{z}}\right|_{\tilde{z}=-\tilde{\varepsilon}\tilde{\eta}}\right) \tag{40}$$

where $|\mathbf{n}| = \sqrt{1+\tilde{\varepsilon}^2\left(\frac{\partial\tilde{\eta}}{\partial\tilde{r}}\right)^2}$.

Using Taylor expansions of $\partial\tilde{T}_0/\partial\tilde{r}$ and $\partial\tilde{T}_0/\partial\tilde{z}$ about $\tilde{z} = 0$

$$\left.\frac{\partial\tilde{T}_0}{\partial\tilde{r}}\right|_{\tilde{z}=-\tilde{\varepsilon}\tilde{\eta}} = \left.\frac{\partial\tilde{T}_0}{\partial\tilde{r}}\right|_{\tilde{z}=0} + O(\tilde{\varepsilon}) \tag{41}$$

$$\left.\frac{\partial\tilde{T}_0}{\partial\tilde{z}}\right|_{\tilde{z}=-\tilde{\varepsilon}\tilde{\eta}} = \left.\frac{\partial\tilde{T}_0}{\partial\tilde{z}}\right|_{\tilde{z}=0} - \tilde{\varepsilon}\tilde{\eta}\left.\frac{\partial^2\tilde{T}_0}{\partial\tilde{z}^2}\right|_{\tilde{z}=0} + O(\tilde{\varepsilon}^2) \tag{42}$$

Substituting Eq. (41), Eq. (42) and $|\mathbf{n}| = 1 + O(\tilde{\varepsilon}^2)$, Eq. (40) becomes

$$\begin{aligned}\left.\frac{\partial \tilde{T}_0}{\partial \hat{n}}\right|_{\tilde{z}=-\tilde{\varepsilon}\tilde{\eta}} = \Bigg[& \tilde{\varepsilon}\frac{\mathrm{d}\tilde{\eta}}{\mathrm{d}\tilde{r}}\left(\left.\frac{\partial \tilde{T}_0}{\partial \tilde{r}}\right|_{\tilde{z}=0} + O(\tilde{\varepsilon})\right) \\ & + \left.\frac{\partial \tilde{T}_0}{\partial \tilde{z}}\right|_{\tilde{z}=0} + -\tilde{\varepsilon}\tilde{\eta}\left.\frac{\partial^2 \tilde{T}_0}{\partial \tilde{z}^2}\right|_{\tilde{z}=0} + O(\tilde{\varepsilon}^2)\Bigg]\end{aligned} \tag{43}$$

However, since the integral is evaluated outside of the contact spot, $\left.\partial \tilde{T}_0/\partial \tilde{z}\right|_{\tilde{z}=0} = 0$, and Eq. (43) becomes

$$\left.\frac{\partial \tilde{T}_0}{\partial \hat{n}}\right|_{\tilde{z}=-\tilde{\varepsilon}\tilde{\eta}} = \tilde{\varepsilon}\left(\frac{d\tilde{\eta}}{d\tilde{r}}\left.\frac{\partial \tilde{T}_0}{\partial \tilde{r}}\right|_{\tilde{z}=0} - \tilde{\eta}\left.\frac{\partial^2 \tilde{T}_0}{\partial \tilde{z}^2}\right|_{\tilde{z}=0}\right) + O(\tilde{\varepsilon}^2) \tag{44}$$

Also, Taylor expanding $\tilde{T}_0$ about $\tilde{z} = 0$

$$\left.\tilde{T}_0\right|_{\tilde{z}=-\tilde{\varepsilon}\tilde{\eta}} = \left.\tilde{T}_0\right|_{\tilde{z}=0} + O(\tilde{\varepsilon}) \tag{45}$$

Then,

$$\left(\left.\tilde{T}_0\right|_{\tilde{z}=-\tilde{\varepsilon}\tilde{\eta}} + \tilde{\varepsilon}\left.\tilde{T}_1\right|_{\tilde{z}=-\tilde{\varepsilon}\tilde{\eta}}\right)\left.\frac{\partial \tilde{T}_0}{\partial \hat{n}}\right|_{\tilde{z}=-\tilde{\varepsilon}\tilde{\eta}} = \tilde{\varepsilon}\left.\tilde{T}_0\right|_{\tilde{z}=0}\left(\frac{\mathrm{d}\tilde{\eta}}{\mathrm{d}\tilde{r}}\left.\frac{\partial \tilde{T}_0}{\partial \tilde{r}}\right|_{\tilde{z}=0} - \tilde{\eta}\left.\frac{\partial^2 \tilde{T}_0}{\partial \tilde{z}^2}\right|_{\tilde{z}=0}\right) + O(\tilde{\varepsilon}^2) \tag{46}$$

i.e., we can ignore $\tilde{T}_1$ to the first-order in $\tilde{\varepsilon}$. Using Eqs. (46) and $\mathrm{d}A = 2\pi\tilde{r}\,\mathrm{d}\tilde{r}$

$$\iint_{\tilde{z}=-\tilde{\varepsilon}\tilde{\eta}} (\tilde{T}_0 + \tilde{\varepsilon}\tilde{T}_1 - 1)\frac{\partial \tilde{T}_0}{\partial \hat{n}}\mathrm{d}A = 2\pi\tilde{\varepsilon}\int_{\phi}^{1} \tilde{r}\left(\left.\tilde{T}_0\right|_{\tilde{z}=0} - 1\right)\left(\frac{\mathrm{d}\tilde{\eta}}{\mathrm{d}\tilde{r}}\left.\frac{\partial \tilde{T}_0}{\partial \tilde{r}}\right|_{\tilde{z}=0} - \tilde{\eta}\left.\frac{\partial^2 \tilde{T}_0}{\partial \tilde{z}^2}\right|_{\tilde{z}=0}\right)\mathrm{d}\tilde{r} + O(\tilde{\varepsilon}^2) \tag{47}$$

Thus, substituting Eq. (47) into Eq. (39) gives

$$\Delta\tilde{T}_{\mathrm{c}} - \Delta\tilde{T}_{0,\mathrm{c}} = 2\tilde{\varepsilon}\tilde{R}''_{\mathrm{sp},0}\int_{\phi}^{1} \tilde{r}\left(\left.\tilde{T}_0\right|_{\tilde{z}=0} - 1\right)\left(\frac{\mathrm{d}\tilde{\eta}}{\mathrm{d}\tilde{r}}\left.\frac{\partial \tilde{T}_0}{\partial \tilde{r}}\right|_{\tilde{z}=0} - \tilde{\eta}\left.\frac{\partial^2 \tilde{T}_0}{\partial \tilde{z}^2}\right|_{\tilde{z}=0}\right)\mathrm{d}\tilde{r} + O(\tilde{\varepsilon}^2) \tag{48}$$

3.2.4 Solution for Spreading and Contact Resistances

From our prescription of dimensionless heat flux as $1/\tilde{R}''_{\mathrm{sp},0}$, then $\tilde{R}''_{\mathrm{sp}} = \Delta\tilde{T}_{\mathrm{c}}\tilde{R}''_{\mathrm{sp},0}$ and we can solve dimensionless spreading resistance in a non-flat contact such that

$$\tilde{R}''_{\mathrm{sp}} = \tilde{R}''_{\mathrm{sp},0} + 2\tilde{\varepsilon}\left(\tilde{R}''_{\mathrm{sp},0}\right)^2 \int_{\phi}^{1} \tilde{r}\left(\left.\tilde{T}_0\right|_{\tilde{z}=0} - 1\right)\left(\frac{\mathrm{d}\tilde{\eta}}{\mathrm{d}\tilde{r}}\left.\frac{\partial\tilde{T}_0}{\partial\tilde{r}}\right|_{\tilde{z}=0} - \tilde{\eta}\left.\frac{\partial^2\tilde{T}_0}{\partial\tilde{z}^2}\right|_{\tilde{z}=0}\right)\mathrm{d}\tilde{r} + O(\tilde{\varepsilon}^2) \tag{49}$$

The integral can be evaluating, with $g(\phi)$ and $h(\phi)$ given in Appendix B

$$\tilde{R}''_{\mathrm{sp}} = \tilde{R}''_{\mathrm{sp},0} + 2\tilde{\varepsilon}\left(\tilde{R}''_{\mathrm{sp},0}\right)^2 [g(\phi) - h(\phi)] \tag{50}$$

This gives the expansion

$$\tilde{R}''_{\mathrm{sp}} = \tilde{R}''_{\mathrm{sp},0} + \tilde{\varepsilon}\tilde{R}''_{\mathrm{sp},1} + O(\tilde{\varepsilon}^2) \tag{51}$$

with

$$\tilde{R}''_{\mathrm{sp},1} = 2(\tilde{R}''_{\mathrm{sp},0})^2 [g(\phi) - h(\phi)] \tag{52}$$

It is important to note that for a contact angle of 0, corresponding to a flat contact, $\tilde{\varepsilon} = 0$ and we retrieve the flat contact solution. The dimensional spreading resistance is given by

$$R''_{\mathrm{sp}} = \frac{b}{k}\tilde{R}''_{\mathrm{sp}} \tag{53}$$

From this we can calculate an expression for R''_{tc} by adding two spreading resistance in series such that

$$R''_{\mathrm{tc}} = \frac{2b}{k}\tilde{R}''_{\mathrm{sp}}$$

where

$$\frac{1}{k} = \frac{1}{2}\left(\frac{1}{k_1} + \frac{1}{k_2}\right) \tag{54}$$

where k_1 and k_2 are the thermal conductivities of the contacting materials 1 and 2 respectively and c and b are the contact spot radius and tube radius respectively. Often, this dimensional thermal

contact resistance expression of a single contact is written as a heat transfer contact conductance coefficient h_c [5] such that

$$h_c = \frac{1}{R''_{\text{tc}}} \tag{55}$$

4 Results

In the flat contact problem (0°), the adiabatic annulus on the base imposes a restriction on the heat flow between the contacting cylinders. As constriction ratio is decreased, the constriction of heat flow increases and thus spreading resistance increases. To solve the flat contact problem we numerically evaluated the requried integrals to generate a 15000-by-15000 matrix used to solve for 500 C_n for 1000 evenly spaced constriction ratios in $0 < \phi < 1$. Using these calculated coefficients, we then evaluated Eq. (49) for different contact angles in the same domain. Dimensionless spreading resistance against constriction ratio is plotted in Fig. 5 for a range of contact angles from -30° to 30°. In is worth noting that negative contact angles are not relevant to contact resistance, but are included for completeness. In the limit as $\phi \to 0$, the resistance asymptotes to resemble that of an adiabatic boundary at $\tilde{z} = 0$, i.e, infinite resistance to heat flow. Conversely, in the limit as $\phi \to 1$, spreading resistance disappears, indicating all resistance to heat flow is one dimensional. As the shape of the contacting cylinders is perturbed from the flat state, the spreading resistance is noticeably affected. For arc protrusion into the cylinder, corresponding to $\alpha > 0^\circ$, the total available volume for heat flow is decreased, increasing spreading resistance. Conversely, for $\alpha < 0^\circ$, the available volume for heat transfer is increased, decreasing spreading resistance. Notably, the effect of non-flatness is most apparent for lower constriction ratios, showing a 15% increase when compared to the flat contact for $\alpha = 20^\circ$ at $\phi = 0.01$. For $0.1 \leq \phi \leq 0.2$, the domain of constriction ratios that most contacts demonstrate [7], and $\alpha = 5^\circ$, we see a notable increase in spreading resistance compared to a flat contact of approximately 3.5% when $\phi = 0.1$ and 3.4% when $\phi = 0.2$. For $\alpha = 20^\circ$, we see a significant increase of approximately 13% when $\phi = 0.1$ and 11% when $\phi = 0.2$. This significant increase highlights the importance of including contact geometry when calculating contact resistance.

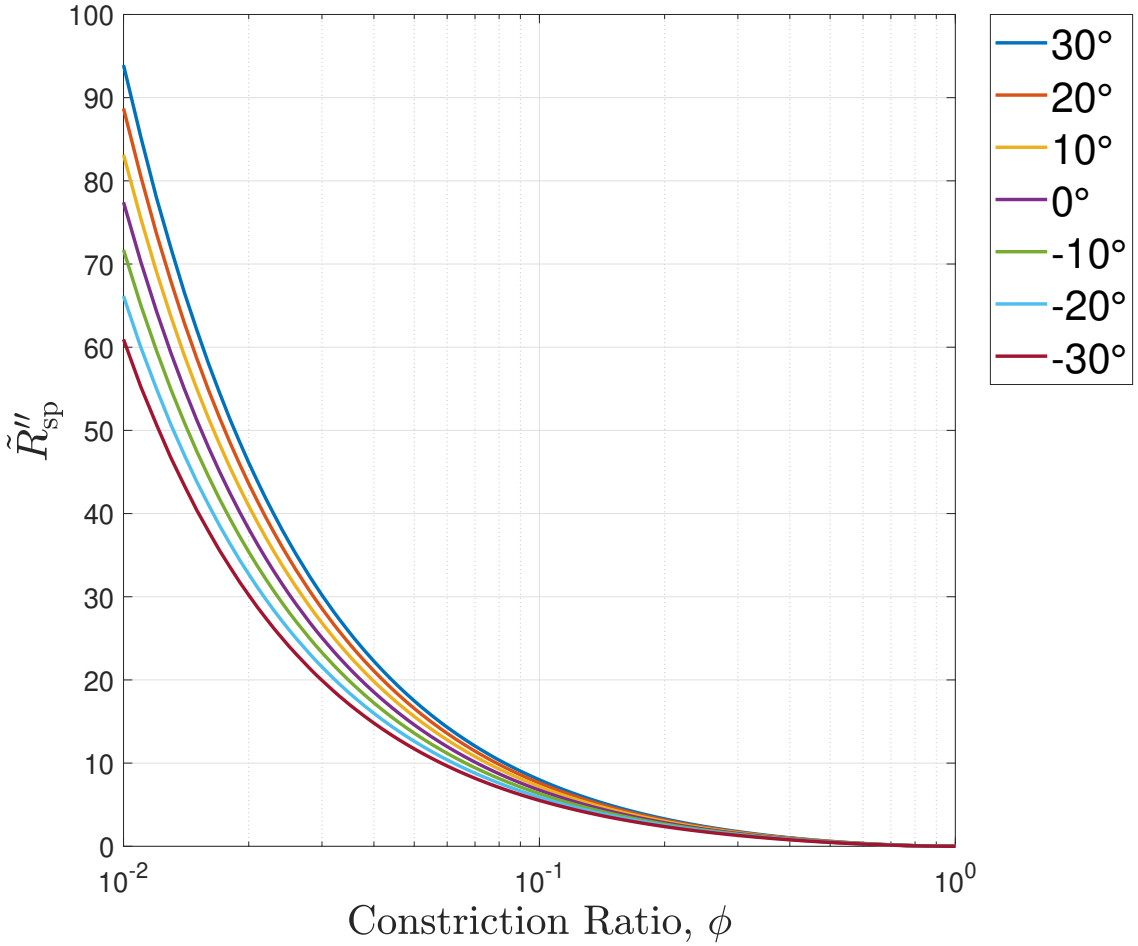

Figure 5: Dimensionless spreading resistance versus constriction ratio, ϕ, for selected contact angles, α.

Additionally, we see good agreement with the numerical results from Madhusudana [13] in their analysis of conical-tipped cylindrical contacts with adiabatic gaps for smallϕ and α. For their geometry corresponding to a contact angle of $\alpha = 22.5^\circ$, they report a dimensionless spreading resistance of around 8 for $\phi = 0.1$ and around 2.4 for $\phi = 0.25$ as per Fig 3 in their paper. Our analytic method gives $\tilde{R}''_{sp} = 7.70$ for $\phi = 0.1$ and $\tilde{R}''_{sp} = 2.30$ for $\phi = 0.1$, differences of 4.00% and 4.35% respectively. This agreement is especially expected at smaller contact angle because the parabolic shape of our adiabatic-arc geometry closely resembles the conical shape of the contacts in [13].

4.1 Model Validation

We validated our asymptotic model, and extended it to arbitrary contact angle, using the finite element method. The partial differential equation solver in MATLAB was used to compute the dimensionless temperature field in the solid domain with the adiabatic-arc, $\tilde{T}_{PDE}$. The dimensionless temperature field was compared to that of the 1-D problem, $\tilde{T}_{1D}$, to find spreading resistance as per Eq. (8) such that

$$\tilde{R}''_{sp,PDE} = \tilde{R}''_{t,PDE} - \tilde{R}''_{1D,PDE} = \tilde{R}''_{sp,0}\left[\left(\tilde{T}_{PDE,source} - \tilde{T}_{PDE,\infty}\right) - \left(\tilde{T}_{1D,source} - \tilde{T}_{1D,\infty}\right)\right]$$

The axisymmetric Laplace equation with relevant boundary conditions was solved with the finite element solver. The domain was discretized with an average of 500,000 elements. The mesh was adapted and refined multiple times to ensure mesh independence and until the difference in temperature drop between subsequent iterations was less than 0.001.

Table 1 compares dimensionless spreading resistance obtained in the perturbation method, $\tilde{R}''_{sp}$, to dimensionless spreading resistance obtained from the partial differential equation solver, $\tilde{R}''_{sp,PDE}$.

ϕ	α	$\tilde{\varepsilon}$	$\tilde{R}''_{\text{sp}}$	$\tilde{R}''_{\text{sp,PDE}}$	Percent Diff.
0.01	20	0.17	88.8	92.5	-4.21
0.01	15	0.13	86.0	87.9	-2.24
0.01	10	0.09	83.2	84.0	-0.93
0.01	5	0.04	80.3	80.5	-0.19
0.01	-5	-0.04	74.5	74.9	-0.49
0.01	-10	-0.09	71.7	72.6	-1.24
0.01	-15	-0.13	68.8	70.6	-2.53
0.01	-20	-0.17	66.1	68.7	-4.04
0.1	20	0.19	7.60	7.85	-3.26
0.1	15	0.14	7.39	7.52	-1.74
0.1	10	0.10	7.18	7.23	-0.73
0.1	5	0.05	6.97	6.98	-0.15
0.1	-5	-0.05	6.53	6.54	-0.16
0.1	-10	-0.10	6.32	6.36	-0.63
0.1	-15	-0.14	6.12	6.2	-1.35
0.1	-20	-0.19	5.90	6.04	-2.32
0.25	20	0.23	2.27	2.33	-2.53
0.25	15	0.17	2.22	2.25	-1.36
0.25	10	0.12	2.16	2.17	-0.56
0.25	5	0.06	2.11	2.11	-0.11
0.25	-5	-0.06	2.00	2.00	-0.11
0.25	-10	-0.12	1.94	1.95	-0.48
0.25	-15	-0.17	1.89	1.91	-1.04
0.25	-20	-0.23	1.83	1.86	-1.64

Table 1: Comparison of perturbaton method values, $\tilde{R}''_{\text{sp}}$, to numerical values, $\tilde{R}''_{\text{sp,PDE}}$

Percent difference is calculated as $100\times[(\tilde{R}''_{\text{sp}} - \tilde{R}_{\text{sp,PDE}})/\tilde{R}''_{\text{sp}}]$ such that percent difference is neg-

ative when $\tilde{R}''_{sp} < \tilde{R}_{sp,PDE}$. This happens when our asymptotic model *underestimates* spreading resistance. We note that the perturbation analysis is expected to break down as the magnitude of $\tilde{\varepsilon}$ increases due to increasing contact angle and solid fraction, i.e., that

$$\tilde{R}''_{sp,PDE} = \tilde{R}''_{sp} + O(\tilde{\varepsilon}^2)$$

As expected we see excellent agreement with the analytical result for small contact angle and increasing divergence for larger values of $\tilde{\varepsilon}$. Figure 6 compares dimensionless spreading resistance from our two models for the $0.1 < \phi < 0.25$, a range that captures the typical range of constriction ratios for contact resistance problems [7]. After validating our model with numerical simulation for small $\tilde{\varepsilon}$, we also use the model to show when our analytical model diverges from the numerical model. Figure 7 depicts Fig. 5 with numerics included. It is clear that the numerical model matches our model fairly well for $\alpha < 20^\circ$, but at $\alpha = 30^\circ$ and above it begins to diverge, with $\alpha = 30^\circ$ showing around a 10% error.

We use the numerical simulation to extend the spreading resistance results to include contact angles of up to both -90 and 90 degrees, completing the parameter space. Figure 8 depicts dimensionless spreading resistance for large positive angles up to 90 degrees, revealing a very large increase in thermal resistance at high contact angles. As $\alpha \to 90^\circ$, the cross section of the adiabatic-arc becomes the bottom half of a circle. Thus the adiabatic surface formed by this perturbed arc constricts heat flow for greater distances from the source plane than for lesser contact angles. This helps explain large asymptotic growth in $\tilde{R}''_{PDE}$ as $\phi \to 0$. Figure 9 shows dimensionless spreading resistance for contact angles from -40 degrees to -90 degrees, showing a significant alleviation of spreading resistance at large negative angles due to the increase in overall volume available for heat transfer.

5 Conclusions

We have developed analytical thermal spreading expressions for a single contact for realistic contact geometries accounting for the non-flat nature of real contacts. The analytical model is applicable

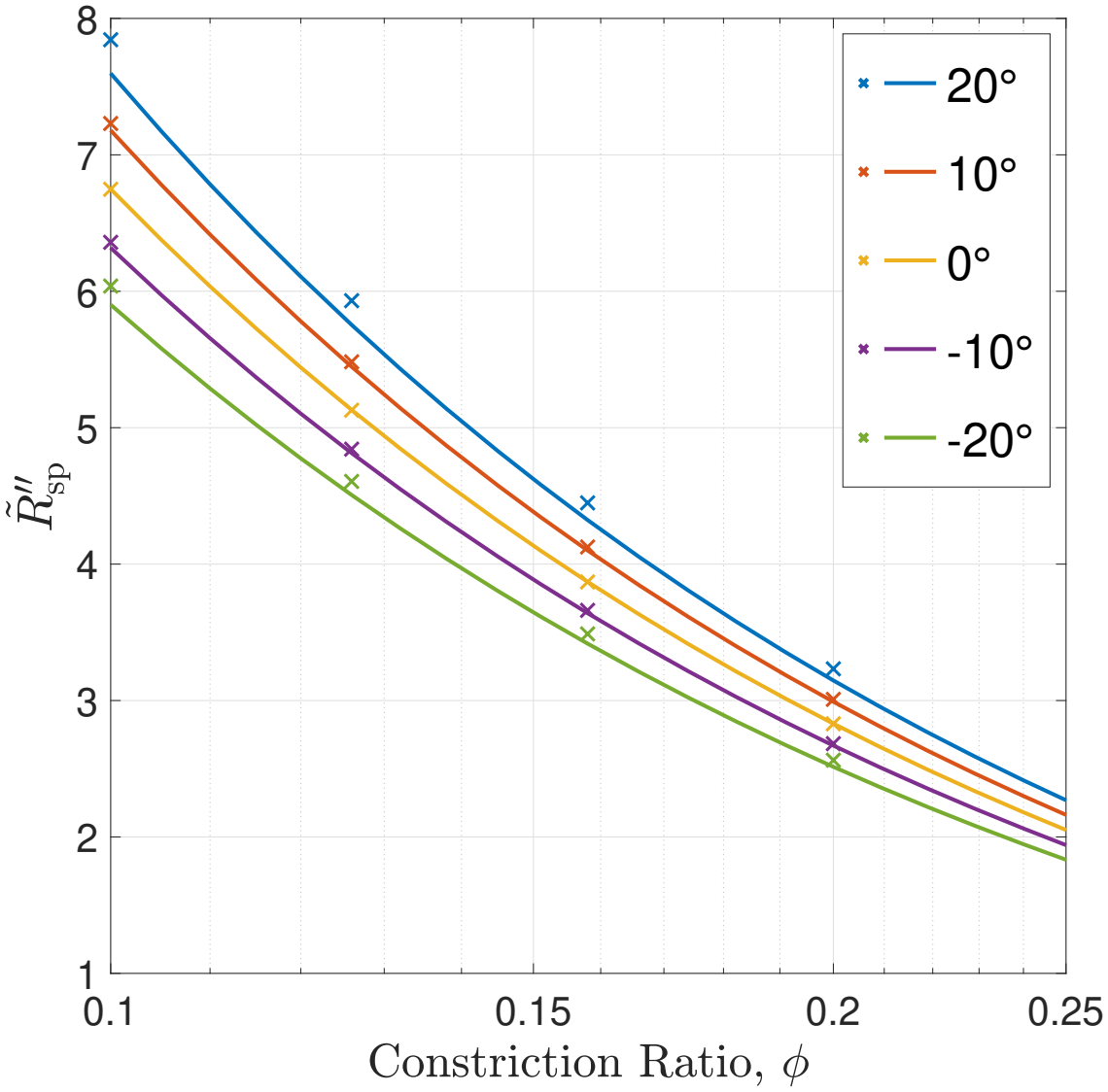

Figure 6: Dimensionless spreading resistance (solid lines) plotted with numerical results (x) for range of constriction ratio and contact angle found in real contacts.

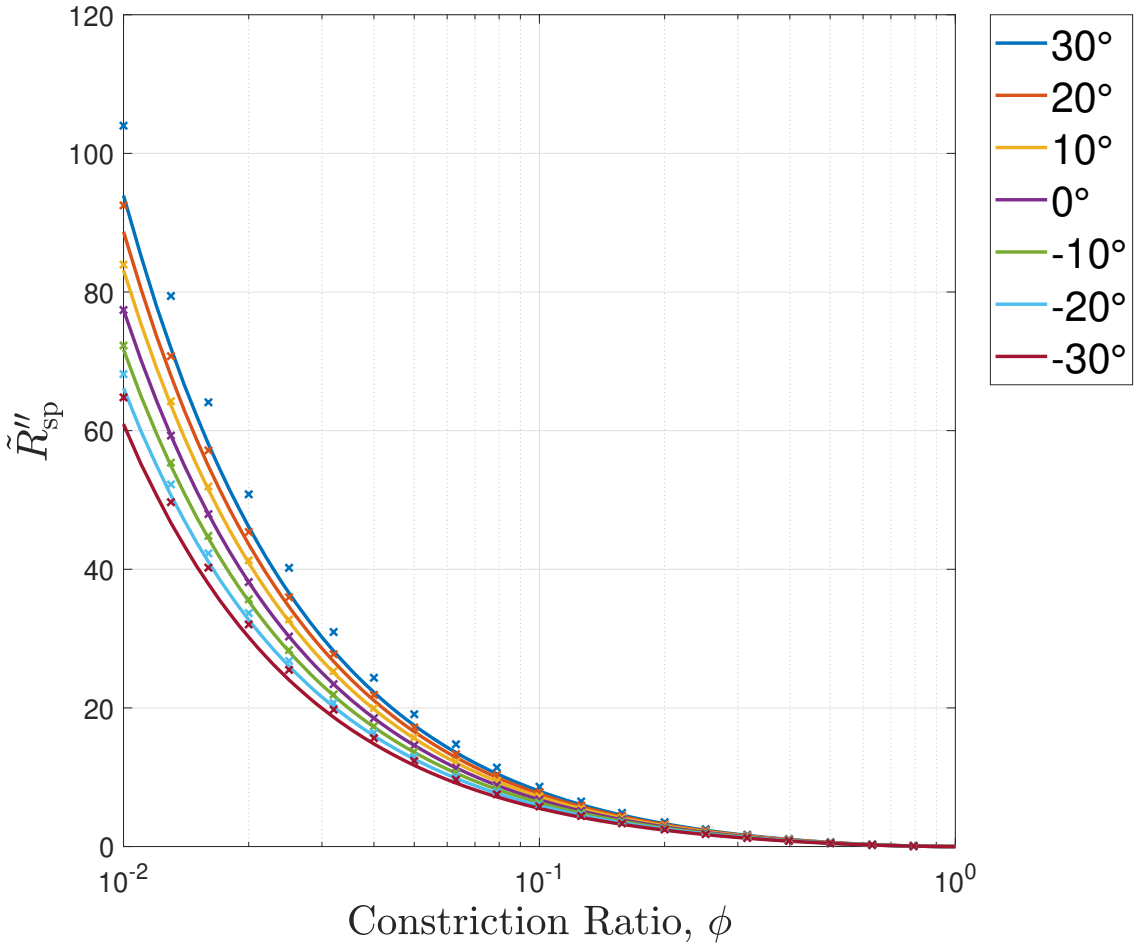

Figure 7: Dimensionless spreading resistance (solid lines) plotted with numerical results (x).

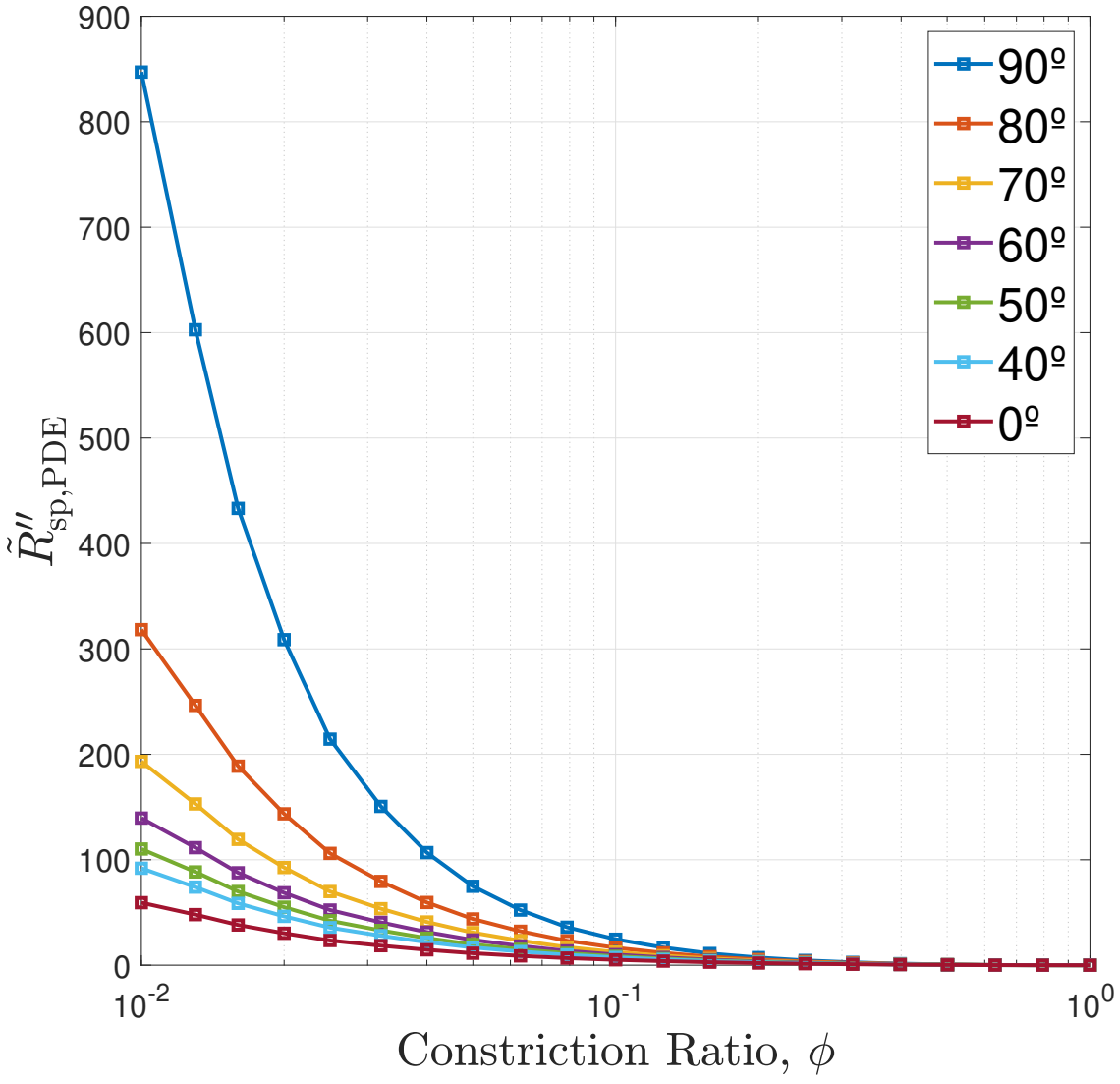

Figure 8: Dimensionless spreading resistance calculated numerically for contact angles higher than 40 degrees.

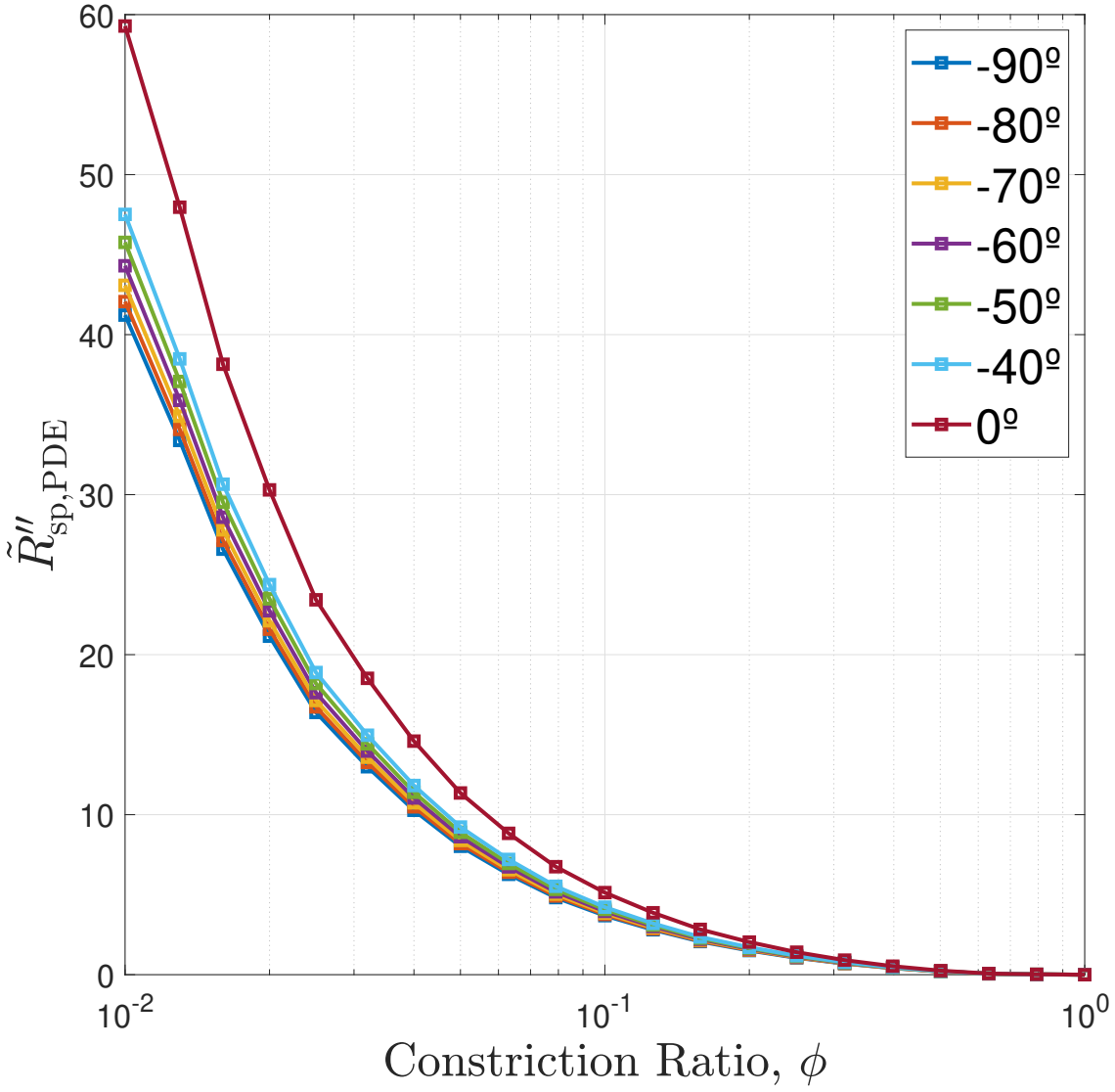

Figure 9: Dimensionless spreading resistance calculated numerically for contact angles less than negative 40 degrees.

for a range of small protrusion angles and constriction ratios which are typical in the contact geometries generated between contacting materials after machining [7, 22]. Our model shows that small perturbations from a flat contact can have significant effects on spreading resistance. Importantly, the non-flatness of contacts has the most significant effect on contact resistance at lower constriction ratios, relevant to real surfaces. In addition, we conducted a finite element simulations that validate our analytical results for small contact angle and constriction ratios. We use the numerical simulation to complete the parameter space, evaluating spreading resistance for arbitrary contact angles and constriction ratios. Constriction ratios and contact angles follow from modelling and measurement used in existing models for contact resistance. Thus, our expressions can be easily implemented into existing models to allow for better estimation of contact resistance and better design of engineering systems in which contact resistance is important. Further work is needed to include the presence of a conducting fluid in the gap, as well as determine the effect of interactions between neighboring contacts on the overall contact resistance.

6 Appendix A: Separation of Variables Solution to Non-Flat Contact

The governing equation is Laplace's with the following boundary conditions

$$\tilde{z}=0 \quad \begin{cases} \tilde{T}_0 = 1 & 0 \le r < \phi \\ \frac{\partial \tilde{T}_0}{\partial \tilde{z}} = 0 & \phi < r \le 1 \end{cases} \tag{56}$$

$$\frac{\partial \tilde{T}_0}{\partial \tilde{z}} = -\frac{1}{\tilde{R}''_{\mathrm{sp}}} \quad \tilde{z} \to \infty \tag{57}$$

$$\frac{\partial \tilde{T}_0}{\partial \tilde{r}} = 0 \quad \tilde{r} = 1 \tag{58}$$

Assuming $\tilde{T}_0 = \sum_{n=1}^{\infty} R_n(\tilde{r})Z_n(\tilde{z})$ we can plug into Laplace's Equation such that

$$\nabla^2 \left[\sum_{n=1}^{\infty} R_n(\tilde{r})Z_n(\tilde{z}) \right] = 0 \rightarrow \frac{1}{\tilde{r}} \frac{\partial}{\partial \tilde{r}} \left(\tilde{r} \frac{\partial \left[\sum_{n=1}^{\infty} R_n(\tilde{r})Z_n(\tilde{z}) \right]}{\partial \tilde{r}} \right) + \frac{\partial^2 \left[\sum_{n=1}^{\infty} R_n(\tilde{r})Z_n(\tilde{z}) \right]}{\partial \tilde{z}^2} = 0$$

We bring the sum notation and independent functions outside such that

$$\sum_{n=1}^{\infty} \frac{Z(\tilde{z})}{\tilde{r}} \frac{\partial}{\partial \tilde{r}} \frac{\partial}{\partial \tilde{r}} \left(\tilde{r} \frac{\partial \left[R_n(\tilde{r}) \right]}{\partial \tilde{r}} \right) + \sum_{n=1}^{\infty} R_n(\tilde{r}) \frac{\partial^2 \left[Z_n(\tilde{z}) \right]}{\partial \tilde{z}^2} = 0$$

For each n, separating the variables yields

$$\frac{1}{Z(\tilde{z})} \frac{\partial^2 \left[Z_n(\tilde{z}) \right]}{\partial \tilde{z}^2} = -\frac{1}{R(\tilde{r})} \left(\frac{\partial^2 \left[R_n(\tilde{r}) \right]}{\partial \tilde{r}^2} + \frac{1}{\tilde{r}} \frac{\partial \left[R_n(\tilde{r}) \right]}{\partial \tilde{r}} \right) = \lambda_n^2$$

since $R_n(\tilde{r})$ and $Z_n(\tilde{z})$ are independent and where λ_n is a constant. We have two ODES then,

$$\frac{\partial^2 \left[R_n(\tilde{r}) \right]}{\partial \tilde{r}^2} + \frac{1}{\tilde{r}} \frac{\partial \left[R_n(\tilde{r}) \right]}{\partial \tilde{r}} + \lambda_n^2 R_n(\tilde{r}) = 0$$

$$\frac{\partial^2 \left[Z_n(\tilde{z}) \right]}{\partial \tilde{z}^2} = \lambda_n^2 Z_n(\tilde{z})$$

The solutions to these ODEs are known such that when $\lambda_n^2 \neq 0$

$$R_n(\tilde{r}) = C_1 J_0(\lambda_n \tilde{r}) + C_2 Y_0(\lambda_n \tilde{r})$$

where J_0 and Y_0 are the Bessel Functions of the First and Second Kind and

$$Z_n(\tilde{z}) = C_3 \exp(\lambda_n \tilde{z}) + C_4 \exp(-\lambda_n \tilde{z})$$

When $\lambda_n = 0$,

$$R_n(\tilde{r}) = C_5 \log(\tilde{r}) + C_6$$

$$Z_n(\tilde{z}) = C_7 \tilde{z} + C_8$$

We combine our solutions such that

$$\tilde{T}_0(\tilde{r},\tilde{z}) = \sum_{n=1}^{\infty} \left[(C_1 J_0(\lambda_n \tilde{r}) + C_2 Y_0(\lambda_n \tilde{r})) \left(C_3 \exp(\lambda_n \tilde{z}) + C_4 \exp(-\lambda_n \tilde{z}) \right) \right] + (C_5 \log(\tilde{r}) + C_6)(C_7 \tilde{z} + C_8)$$

$\tilde{T}_0(\tilde{r},\tilde{z})$ and its partial derivatives have no singularity at $\tilde{r} = 0$ so $C_2 = C_5 = 0$. Additionally, due to 57 $C_3 = 0$, and $C_7 = -1/\tilde{R}''_{\text{sp}}$. We are left with

$$\tilde{T}_0(\tilde{r},\tilde{z}) = -\frac{1}{\tilde{R}''_{\text{sp}}}\tilde{z} + \sum_{n=1}^{\infty} \left[C_n J_0(\lambda_n \tilde{r}) \exp(-\lambda_n \tilde{z}) \right] + C_8$$

Applying 58, then the eigenvalues satisfy $J_1(\lambda_n) = 0$. Taking the average temperature in a cross section

$$\tilde{T}_{0,\text{avg}} = \frac{1}{\pi} \int_0^1 2\pi r \tilde{T}_0(\tilde{r},\tilde{z}) \mathrm{d}r = -\frac{1}{\tilde{R}''_{\text{sp}}}\tilde{z} + 2\left[\lambda_n^{-1} C_n J_1(\lambda_n) \exp(-\lambda_n \tilde{z}) - \lambda_n^{-1} C_n J_1(0) \exp(-\lambda_n \tilde{z}) \right] + C_8$$

From the eigenvalue condition then,

$$\tilde{T}_{0,\text{avg}} = -\frac{1}{\tilde{R}''_{\text{sp}}}\tilde{z} + C_8$$

and C_8 represents the average temperature on the $\tilde{z} = 0$ plane. Since C_n is an unknown constant, we can

$$\tilde{T}_0(\tilde{r},\tilde{z}) = -\frac{1}{\tilde{R}''_{\text{sp}}}\tilde{z} + \sum_{n=1}^{\infty} \left[\lambda_n^{-1} C_n J_0(\lambda_n \tilde{r}) \exp(-\lambda_n \tilde{z}) \right] + C_8$$

This field satisfies the same boundary conditions as before.

7 Appendix B: Evaluation of Integrals

All integrals were evaluated from solutions to integral solutions to combinations of various Bessel functions as given by [1]. The integrals in the evaluation below were evaluated numerically during calculations

$$\tilde{T}_0\big|_{\tilde{z}=0} = \sum_{n=1}^{\infty} \lambda_n^{-1} C_n J_0(\lambda_n \tilde{r})$$

$$\left.\frac{\partial \tilde{T}_0}{\partial \tilde{r}}\right|_{\tilde{z}=0} = -\sum_{n=1}^{\infty} C_n J_1(\lambda_n \tilde{r})$$

$$\left.\frac{\partial^2 \tilde{T}_0}{\partial \tilde{z}^2}\right|_{\tilde{z}=0} = \sum_{n=1}^{\infty} \lambda_n C_n J_0(\lambda_n \tilde{r})$$

$$\tilde{\eta} = (\tilde{r}-1)^2 - (1-\phi)^2 = \tilde{r}^2 - 2\tilde{r} + 2\phi - \phi^2$$

$$\frac{d\tilde{\eta}}{d\tilde{r}} = 2\tilde{r} - 2$$

$$g(\phi) = \int_{\phi}^{1} \tilde{r} \left(\tilde{T}_0\big|_{\tilde{z}=0} \right) \left(\frac{d\tilde{\eta}}{d\tilde{r}} \left.\frac{\partial \tilde{T}_0}{\partial \tilde{r}}\right|_{\tilde{z}=0} - \tilde{\eta} \left.\frac{\partial^2 \tilde{T}_0}{\partial \tilde{z}^2}\right|_{\tilde{z}=0} \right) \mathrm{d}\tilde{r}$$

$$\begin{aligned} g(\phi) = \sum_{m=1}^{\infty} C_m \lambda_m^{-1} \sum_{n=1}^{\infty} C_n \{ & -2 \int_{\phi}^{1} \tilde{r} J_0(\lambda_m \tilde{r}) J_1(\lambda_n \tilde{r}) \mathrm{d}\tilde{r} \\ & + 2 \int_{\phi}^{1} \tilde{r}^2 J_0(\lambda_m \tilde{r}) J_1(\lambda_n \tilde{r}) \mathrm{d}\tilde{r} \\ & + \lambda_n \Bigg[(2\phi - \phi^2) \int_{\phi}^{1} \tilde{r} J_0(\lambda_m \tilde{r}) J_0(\lambda_n \tilde{r}) \mathrm{d}\tilde{r} \\ & - 2 \int_{\phi}^{1} \tilde{r}^2 J_0(\lambda_m \tilde{r}) J_0(\lambda_n \tilde{r}) \mathrm{d}\tilde{r} \\ & + \int_{\phi}^{1} \tilde{r}^3 J_0(\lambda_m \tilde{r}) J_0(\lambda_n \tilde{r}) \mathrm{d}\tilde{r} \Bigg] \} \end{aligned}$$

$$
\begin{aligned}
g(\phi) = \sum_{m\neq n;m,n=1}^{\infty} \lambda_m^{-1} C_m C_n * \Bigg\{ & -2\Bigg(\frac{\tilde{r}}{\lambda_m^2-\lambda_n^2}[\lambda_n J_0(\lambda_m\tilde{r})J_0(\lambda_n\tilde{r}) + \lambda_m J_1(\lambda_m\tilde{r})J_1(\lambda_n\tilde{r})]\Big|_{\phi}^{1} \\
& - \frac{\lambda_n}{\lambda_m^2-\lambda_n^2}\int_{\phi}^{1} J_0(\lambda_m\tilde{r})J_0(\lambda_n\tilde{r})\mathrm{d}\tilde{r} + \frac{\lambda_m}{\lambda_m^2-\lambda_n^2}\int_{\phi}^{1} J_1(\lambda_m\tilde{r})J_1(\lambda_n\tilde{r})\mathrm{d}\tilde{r}\Bigg) \\
& + 2\Bigg(\frac{2\lambda_n\tilde{r}}{(\lambda_m^2-\lambda_n^2)^2}[\lambda_n J_0(\lambda_m\tilde{r})J_1(\lambda_n\tilde{r}) - \lambda_m J_1(\lambda_m\tilde{r})J_0(\lambda_n\tilde{r})] \\
& + \frac{\tilde{r}^2}{\lambda_m^2-\lambda_n^2}\,[\lambda_n J_0(\lambda_m\tilde{r})J_0(\lambda_n\tilde{r}) + \lambda_m J_1(\lambda_m\tilde{r})J_1(\lambda_n\tilde{r})]\Bigg)\Bigg|_{\phi}^{1} \\
& + \lambda_n\Bigg[(2\phi-\phi^2)\left[\frac{\lambda_m\tilde{r}J_1(\lambda_m\tilde{r})J_0(\lambda_n\tilde{r}) - \lambda_n\tilde{r}J_0(\lambda_m\tilde{r})J_1(\lambda_n\tilde{r})}{\lambda_m^2-\lambda_n^2}\right]\Bigg|_{\phi}^{1} \\
& - 2\Bigg(\Bigg[\frac{\tilde{r}(\lambda_n^2+\lambda_m^2)}{(\lambda_m^2-\lambda_n^2)^2}J_0(\lambda_m\tilde{r})J_0(\lambda_n\tilde{r}) - \frac{\lambda_n\tilde{r}^2}{\lambda_m^2-\lambda_n^2}J_0(\lambda_m\tilde{r})J_1(\lambda_n\tilde{r}) \\
& + \frac{\lambda_m\tilde{r}^2}{\lambda_m^2-\lambda_n^2}J_1(\lambda_m\tilde{r})J_0(\lambda_n\tilde{r}) + 2\frac{\tilde{r}\lambda_n\lambda_m}{(\lambda_m^2-\lambda_n^2)^2}J_1(\lambda_m\tilde{r})J_1(\lambda_n\tilde{r})\Bigg]\Bigg|_{\phi}^{1} \\
& + \frac{\lambda_n^2+\lambda_m^2}{(\lambda_m^2-\lambda_n^2)^2}\int_{\phi}^{1} J_0(\lambda_m\tilde{r})J_0(\lambda_n\tilde{r})\mathrm{d}\tilde{r} - 2\frac{\lambda_n\lambda_m}{(\lambda_m^2-\lambda_n^2)^2}\int_{\phi}^{1} J_1(\lambda_m\tilde{r})J_1(\lambda_n\tilde{r})\mathrm{d}\tilde{r}\Bigg) \\
& + \Bigg(\frac{2\tilde{r}^2}{(\lambda_m^2-\lambda_n^2)^2}[(\lambda_m^2+\lambda_n^2)J_0(\lambda_m\tilde{r})J_0(\lambda_n\tilde{r}) + 2\lambda_m\lambda_n J_1(\lambda_m\tilde{r})J_1(\lambda_n\tilde{r})] \\
& + \left[4\tilde{r}\frac{\lambda_m^2+\lambda_n^2}{(\lambda_m^2-\lambda_n^2)^3} - \frac{\tilde{r}^3}{\lambda_m^2-\lambda_n^2}\right][\lambda_n J_0(\lambda_m\tilde{r})J_1(\lambda_n\tilde{r}) - \lambda_m J_1(\lambda_m\tilde{r})J_0(\lambda_n\tilde{r})]\Bigg)\Bigg|_{\phi}^{1}\Bigg]\Bigg\} \\
+ \sum_{m=n=1}^{\infty} C_n^2\lambda_n^{-1}\{ & -2\left[-\frac{\tilde{r}}{2\lambda_n}J_0^2(\lambda_n\tilde{r})\Big|_{\phi}^{1} + \frac{1}{2\lambda_n}\int_{\phi}^{1} J_0^2(\lambda_n\tilde{r})\mathrm{d}\tilde{r}\right] \\
& + 2\left[\frac{\tilde{r}}{2\lambda_n}J_1(\lambda_n\tilde{r})\Big|_{\phi}^{1}\right] \\
& + \lambda_n\left[(2\phi-\phi^2)\left[\frac{\tilde{r}^2}{2}\left(J_0^2(\lambda_n\tilde{r}) + J_1^2(\lambda_n\tilde{r})\right)\Big|_{\phi}^{1}\right]\right. \\
& - 2\Bigg(\frac{1}{8\lambda_n^3}\,\left[(2\lambda_n\tilde{r}^3+\tilde{r})J_0^2(\lambda_n\tilde{r}) + 2\lambda_n\tilde{r}^2J_0(\lambda_n\tilde{r})J_1(\lambda_n\tilde{r}) + 2\lambda_n^2\tilde{r}^2J_1^2(\lambda_n\tilde{r})\right]\Big|_{\phi}^{1} \\
& - \int_{\phi}^{1} J_0^2(\lambda_n\tilde{r})\mathrm{d}\tilde{r}\Bigg) \\
& + \left.\left(\left(\frac{\lambda_n^2\tilde{r}^4-2\tilde{r}}{\lambda_n^2}\right)J_1^2(\lambda_n\tilde{r}) + \frac{\tilde{r}^3}{3\lambda_n}J_0(\lambda_n\tilde{r})J_1(\lambda_n\tilde{r}) + \frac{\tilde{r}^4}{6}J_0^2(\lambda_n\tilde{r})\right)\Big|_{\phi}^{1}\right]\}
\end{aligned}
$$

$$
h(\phi) = \int_{\phi}^{1} \tilde{r}\left(\frac{d\tilde{\eta}}{d\tilde{r}}\,\frac{\partial\tilde{T}_0}{\partial\tilde{r}}\Big|_{\tilde{z}=0} - \tilde{\eta}\,\frac{\partial^2\tilde{T}_0}{\partial\tilde{z}^2}\Big|_{\tilde{z}=0}\right)\mathrm{d}\tilde{r}
$$

$$h(\phi) = \sum_{n=1}^{\infty} C_n \left[-2\int_{\phi}^{1} \tilde{r} J_1(\lambda_n \tilde{r}) \mathrm{d}\tilde{r} + 2\int_{\phi}^{1} \tilde{r}^2 J_1(\lambda_n \tilde{r}) \mathrm{d}\tilde{r} + \right.$$
$$\left. \lambda_n \left[(2\phi - \phi^2) \int_{\phi}^{1} \tilde{r} J_0(\lambda_n \tilde{r}) \mathrm{d}\tilde{r} - 2\int_{\phi}^{1} \tilde{r}^2 J_0(\lambda_n \tilde{r}) \mathrm{d}\tilde{r} + \int_{\phi}^{1} \tilde{r}^3 J_0(\lambda_n \tilde{r}) \mathrm{d}\tilde{r} \right] \right]$$

$$\begin{aligned}
h(\phi) = \sum_{n=1}^{\infty} C_n * \{ & \\
& -2 \left[\frac{\pi \tilde{r}}{2\lambda_n} \left(J_1(\lambda_n \tilde{r}) H_0(\lambda_n \tilde{r}) - J_0(\lambda_n \tilde{r}) H_1(\lambda_n \tilde{r}) \right) \Big|_{\phi}^{1} \right] \\
& + 2 \left[\frac{\tilde{r}^2 J_2(\lambda_n \tilde{r})}{\lambda_n} \Big|_{\phi}^{1} \right] \\
& + \lambda_n \left[(2\phi - \phi^2) \left(\frac{\tilde{r} J_1(\lambda_n \tilde{r})}{\lambda_n} \Big|_{\phi}^{1} \right) \right. \\
& \left. - 2 \left(\frac{\tilde{r}^2}{\lambda_n} J_1(\lambda_n \tilde{r}) - \left(\frac{\pi}{2\lambda_n^2} \left[J_1(\lambda_n \tilde{r}) H_0(\lambda_n \tilde{r}) - J_0(\lambda_n \tilde{r}) H_1(\lambda_n \tilde{r}) \right] \right) \Big|_{\phi}^{1} \right) \right. \\
& \left. + \frac{\tilde{r}^2 \left(\lambda_n \tilde{r} J_3(\lambda_n \tilde{r}) - 2 J_2(\lambda_n \tilde{r}) \right)}{\lambda_n^2} \Big|_{\phi}^{1} \right] \}
\end{aligned}$$

where H_{n} is the Struve function of the n-th kind.

Nomenclature

Roman Symbols

$\hat{n}$	Unit Normal
b	Cylinder Radius
c	Contact Spot Radius
h_c	Thermal Conductance Coefficient
k	Thermal Conductivity
$k_{1,2}$	Thermal Conductivity of Material 1,2
L	Length
$L_{1,2}$	Length of Material 1,2

Greek Symbols

α	Contact Angle
γ	Contact Fraction
ϕ	Constriction Ratio
$\tilde{\varepsilon}$	Small Parameter (1/2 Arc Curvature)
$\tilde{\eta}$	Shape of Adiabatic Arc

Mathematical Symbols

H_n	n-th Order Struve Function
$\Delta\tilde{T}_{0,\mathrm{c}}$	Dimensionless Temperature Drop due to Constriction (Flat Contact)
$\Delta\tilde{T}_{\mathrm{c}}$	Dimensionless Temperature Drop due to Constriction (Non-Flat Contact)

ΔT	Temperature Drop
ΔT_c	Temperature Drop due to spreading or constricting
$\tilde{R}$	Dimensionless arc radius
$\tilde{R}''_{sp,0}$	Dimensionless Thermal Spreading Resistance Flat Contact
$\tilde{R}''_{sp}$	Dimensionless Thermal Spreading Resistance Non-flat Contact
$\tilde{R}''_{tc}$	Dimensionless Thermal Contact Resistance
$\tilde{R}''_{1D,PDE}$	1D Dimensionless Resistance
$\tilde{R}''_{sp,PDE}$	Dimensionless Spreading Resistance
$\tilde{R}''_{t,PDE}$	Total Dimensionless Resistance
$\tilde{T}$	Dimensionless non-flat Contact Solution
$\tilde{T}_0$	Dimensionless flat Contact Solution
$\tilde{T}_{1D,\infty}$	Dimensionless 1D Far Field Temperature
$\tilde{T}_{1D,source}$	Dimensionless 1D Source Temperature
$\tilde{T}_{1D}$	Dimensionless 1D Temperature Field
$\tilde{T}_{PDE,\infty}$	Dimensionless Non-Flat Far Field Temperature
$\tilde{T}_{PDE,source}$	Dimensionless Non-Flat Source Temperature
$\tilde{T}_{PDE}$	Dimensionless Non-Flat Temperature Field
I_1	Modified Bessel Function of the First Kind
J_0, J_1	Bessel Functions of the First Kind
K_1	Modified Bessel Function of the Second Kind

q''	Heat Flux through Cylinder far from Contact
R	Arc Radius
R''	Flux-based thermal resistance
R''_{1D}	1-D Thermal Resistance
R''_{ideal}	Ideal thermal resistance between contacting materials
R''_{sp}	Spreading resistance
R''_{tc}	Thermal Contact Conductance
R''_{t}	Total Thermal Resistance of the cylinder
T	Non-Flat Contact Solution
T_0	Flat Contact Solution
T_{source}	Contact Spot Temperature

References

[1] W. Rosenheinrich, "Tables of some indefinite integrals of bessel functions," *University of Applied sciences Jenna, Germany*, pp. 276–285, 2012.

[2] B. B. Mikic and W. M. Rohsenow, "Thermal contact resistance," Tech. Rep. September, MIT, 1966.

[3] D. G. Crowdy, "Analytical formulae for longitudinal slip lengths over unidirectional superhydrophobic surfaces with curved menisci," *J. Fluid Mech*, vol. 791, 2018.

[4] M. Hodes, T. Kirk, and D. Crowdy, "Thermal Spreading and Contact Resistance Formulae Capturing Boundary Curvature and Contact Distribution Effects," *Journal of Heat Transfer*, no. 2, 2018.

[5] M. G. Cooper, B. B. Mikic, and M. M. Yovanovich, "Thermal Contact Conductance," *Int. J. Heat Mass Transer*, vol. 12, pp. 279–300, 1969.

[6] A. K. Das and S. S. Sadhal, "The Effect of Interstitial Fluid on Thermal Constriction Resistance," *Journal of Heat Transfer*, vol. 114, p. 1045, nov 1992.

[7] K. Negus and M. Yovanovich, "Constriction Resistance of Circular Flux Tubes with Mixed Boundary Conditions by Linear Superposition of Neumann Solutions," *ASME Paper 84-HT-84*, pp. 1–6, 1984.

[8] A. Hunter and A. Williams, "Heat Flow Across Metallic Joints - The Constriction Alleviation Factor," *Int. J. Heat Mass Transer*, vol. 12, pp. 524–526, 1968.

[9] I. N. Sneddon, *Mixed Boundary Value Problems in Potential Theory*. Amsterdam: North-Holland Publishing Company, 1966.

[10] J. A. Greenwood and J. B. P. Williamson, "Contact of Nominally Flat Surfaces," *Proceedings of the Royal Society A: Mathematical, Physical and Engineering Sciences*, vol. 295, no. 1442, pp. 300–319, 1966.

[11] M. M. Yovanovich, "Four decades of research on thermal contact, gap, and joint resistance in microelectronics," *IEEE Transactions on Components and Packaging Technologies*, vol. 28, pp. 182–206, jun 2005.

[12] M. Razavi, Y. S. Muzychka, and S. Kocabiyik, "Review of Advances in Thermal Spreading Resistance Problems," *Journal of Thermophysics and Heat Transfer*, vol. 30, no. 4, pp. 863–879, 2016.

[13] C. V. Madhusudana, "Heat Flow Through Conical Constrictions," *AIAA Journal*, vol. 18, no. 10, pp. 1261–1262, 1980.

[14] Y. Sano, "Effect of space angle on constriction resistance and contact resistance for a point contact," *Journal of Applied Physics*, vol. 58, no. 7, pp. 2651–2654, 1985.

[15] A. K. Das, *Thermal constriction resistance: Effects of clustering, random distribution and interstitial fluid*. PhD thesis, University of Southern California, 1994.

[16] A. K. Das and S. S. Sadhal, "A Note on the Evaluation of Thermal Constriction Resistance for Finite Thickness Gaps," *Journal of Heat Transfer*, vol. 119, pp. 177–180, 1997.

[17] A. K. Das and S. S. Sadhal, "Analytical solution for constriction resistance with interstitial fluid in the gap," *Heat and Mass Transfer*, vol. 34, no. 2-3, pp. 111–119, 1998.

[18] R. Enright, M. Hodes, T. Salamon, and Y. Muzychka, "Isoflux Nusselt Number and Slip Length Formulae for Superhydrophobic Microchannels," *Journal of Heat Transfer*, vol. 136, no. 1, p. 012402, 2013.

[19] M. Sbragaglia and A. Prosperetti, "A note on the effective slip properties for microchannel flows with ultrahydrophobic surfaces," *Physics of Fluids*, vol. 19, no. 4, pp. 1–8, 2007.

[20] L. Steigerwalt Lam, M. Hodes, G. Karamanis, T. Kirk, and S. MacLachlan, "Effect of Meniscus Curvature on Apparent Thermal Slip," *Journal of Heat Transfer*, vol. 138, no. 12, p. 122004, 2016.

[21] D. G. Crowdy, "Perturbation analysis of subphase gas and meniscus curvature effects for longitudinal flows over superhydrophobic surfaces," *Journal of Fluid Mechanics*, vol. 822, no. 19, pp. 307–326, 2017.

[22] A. Grigoriev, "Slope angles of rough surface asperities after machining," *Journal of Friction and Wear*, vol. 36, no. 3, pp. 197–199, 2015.